ADAPTIVE SPACE-FREQUENCY RAKE RECEIVERS FOR WCDMA

Christopher Brunner,[1,2] *Martin Haardt,*[1] *and Josef A. Nossek* [2]

1. Siemens AG, Mobile Networks, OEN MN P 36
Hofmannstr. 51, D-81359 Munich, Germany
Phone / Fax: +49 (89) 722-39159 / -44958
E-Mail: Martin.Haardt@oen.siemens.de

2. Institute for Network Theory and Circuit Design
Munich Univ. of Technology, D-80290 Munich, Germany
Phone / Fax: +49 (89) 289-28511 / -28504
E-Mail: Christopher.Brunner@ei.tum.de

ABSTRACT

Adaptive space-frequency rake receivers use maximum ratio combining and multi-user interference suppression to obtain a considerable increase in performance in DS-CDMA systems such as WCDMA. To this end, the signal-plus-interference-and-noise and the interference-plus-noise space-time covariance matrices are estimated. The computational complexity is reduced significantly by transforming the covariance matrices into the space-frequency domain and by omitting noisy space-frequency bins. The optimum weight vector for symbol decisions is the "largest" generalized eigenvector of the resulting matrix pencil. By iteratively updating the optimum weight vector slot by slot, real-time applicability becomes feasable while the fast fading is still tracked. The performance and the computational complexity depend on the number of space-frequency bins, antenna elements, and iterations. Therefore, the performance can easily be scaled with respect to the available computational power.

1. INTRODUCTION

Adaptive antennas exploit the inherent spatial diversity of the mobile radio channel and are, therefore, seen as an important technology to meet the high spectral efficiency and quality requirements of third generation mobile radio systems. The proposed concepts for the third generation [3] allow an easy and flexible implementation of new and more sophisticated services. Recently, ETSI SMG selected the TD-CDMA concept as the radio access scheme for time-division duplex systems and the WCDMA concept for frequency-division duplex systems [1].

The main advantage of the conventional space-time rake [4] for single-user data detection is its simplicity. However, in scenarios with considerable delay spread, signal energy is lost since the number of rake fingers is limited. Worse, since co-channel interferers are not taken into account, the conventional space-time rake is not near-far resistent. A space-time rake based on space-time covariance matrices combines each multipath across space and time, performs multi-user interference suppression in addition to maximum ratio combining, and, therefore, mitigates the stringent power control requirements common to DS-CDMA systems. Hence, a direct capacity increase is achieved on the uplink [2] by transmitting more codes with lower spreading factors. Due to the reduced transmission rate for uplink power control due to mitigated power control requirements, the downlink capacity for data transmission is also increased. In [6], a blind space-frequency rake receiver was presented by Zoltowski *et al.* Our approach is not blind since we use pilot symbols on the dedicated physical control channel (PCCH) [3] to estimate the covariance matrices and the optimum weight vector. Then we also apply the optimum weight vector to the dedicated physical data channel (PDCH) [3] for symbol detection. The space-frequency rake receiver operates on space-frequency covariance matrices. By omitting noisy space-frequency bins, the computational complexity is reduced. Alternatively, we can also operate in the beamspace-frequency domain, e.g., if the directions of arrival (DOAs) of interest are restricted to a certain spatial sector.

This paper is organized as follows. Taking into account the uplink channel structure of WCDMA, which is described in Section 2, we explain the estimation of the signal-plus-interference-and-noise (SIN) covariance matrix along with the interference-plus-noise (IN) covariance matrix and the tracking of the optimum weight vector in Section 3. The conventional space-time rake receiver, the space-frequency rake receiver, and the beamspace-frequency rake receiver are explained in Section 4. Section 5 compares the different rake receivers by means of Monte-Carlo simulations with respect to performance and computational complexity.

2. WCDMA UPLINK CHANNEL STRUCTURE

WCDMA has two types of dedicated physical channels on the uplink (and the downlink), the PCCH and the PDCH. In case of low and medium data rates, one connection consists of one PCCH and one PDCH [3]. The PDCH baseband signal of the user of interest may be expressed as

$$s_{\mathrm{D}}(t) = \sum_{\ell=-\infty}^{\infty} b_{\mathrm{D}}^{(\ell)}\, z_{\mathrm{D}}(t-\ell T_{\mathrm{D}}), \quad z_{\mathrm{D}}(t) = \sum_{m=1}^{n_{\mathrm{D}}} d_{\mathrm{D}}^{(m)}\, p(t-mT_c).$$

The chip rate in WCDMA is $1/T_c = 4.096$ Mchips/s. Moreover, the spreading sequence of the PDCH, $z_{\mathrm{D}}(t)$, is of length $T_{\mathrm{D}} = n_{\mathrm{D}} T_c$ and is composed of n_{D} chips $d_{\mathrm{D}}^{(m)} \in \{-1,1\}, 1 \le m \le n_{\mathrm{D}}$. The symbols, $b_{\mathrm{D}}^{(\ell)} \in \{-1,1\}$, are BPSK modulated. WCDMA uses a chip waveform, $p(t) \in \mathbb{R}$, characterized by a square-root raised cosine spectrum with a rolloff factor of $\alpha = 0.22$.

The PCCH baseband signal, $s_{\mathrm{C}}(t)$, can be expressed in the same way. A combination of code and IQ multiplexing is used on the uplink, cf. Figure 1, where the PDCH and the PCCH are spread by different spreading codes [3] and mapped to the I and Q branches, respectively, according to

$$s(t) = s_{\mathrm{D}}(t) + \mathrm{j} \cdot s_{\mathrm{C}}(t).$$

[1] This solution has been contributed to the International Telecommunication Union - as the European candidate for IMT-2000 transmission technology.

[2] Here, adaptive antennas are only assumed at base stations. Our scheme, however, also applies to mobiles with adaptive antennas.

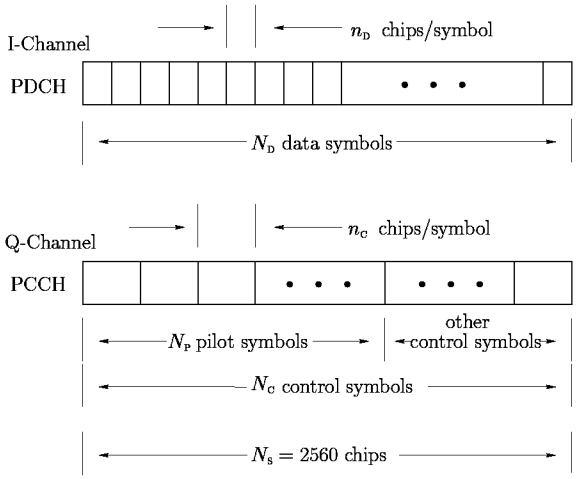

Figure 1: Uplink slot structure of WCDMA: A combination of code and IQ multiplexing is used. Moreover, N_P pilot symbols are transmitted at the beginning of each PCCH slot.

Next, the complex I + jQ signal is either scrambled by a complex short code (256 chips) or by a complex long code (40960 chips) [3]. For simplicity, we do not include scrambling in our notation. In the simulation runs, long scrambling codes were used.

3. GENERATION OF THE COVARIANCE MATRICES

We assume that the receiver is synchronized to the beginning of a slot. Then the (over)sampled output of each antenna element is passed through a correlator of N_P pilot symbols [3]

$$c_P(nT_I) = \sum_{\ell=0}^{N_P-1} b_C^{(\ell)}\, z_C(nT_I - \ell T_C), \tag{1}$$

cf. Figure 2. Let each row of $\mathcal{X}_P \in \mathbb{C}^{M\times(N_s M_c)}$ contain $N_s M_c$ samples of the output of the corresponding antenna element after the correlator, where the oversampling factor and the number of antenna elements are denoted by $M_c = T_C/T_I$ and M, respectively. Next, a selection matrix

$$\boldsymbol{J}^{(i)} = \begin{bmatrix} \mathbf{0}_{(i-1)\times N_w} \\ \boldsymbol{I}_{N_w\times N_w} \\ \mathbf{0}_{(N_s M_c - i - N_w + 1)\times N_w} \end{bmatrix}$$

is applied to the correlator output $\mathcal{X}_P$ such that $\mathcal{X}_P\boldsymbol{J}^{(i)} \in \mathbb{C}^{M\times N_w}$ contains all multipath components for $i = 1$. The length of the delay spread of the user of interest (in samples) is denoted by $N_w = M_c\frac{\tau_{max}}{T_c}$. For $i = N_w, N_w+1, ..., N_s M_c - N_w$, the selection matrix acts as a sliding window. Its outputs $\mathcal{X}_P\boldsymbol{J}^{(i)}$ are averaged to estimate the space-frequency IN covariance matrix. To this end, we define the ith space-time snapshot as $\boldsymbol{y}_P^{(i)} = \text{vec}\left\{\mathcal{X}_P\boldsymbol{J}^{(i)}\right\}$. The vec-operator maps an $m \times n$ matrix into an mn-dimensional column vector by stacking the columns of the matrix. A space-frequency transformation is performed by post-multiplying the selected correlation output with the N_w-point DFT matrix $\boldsymbol{W}_T$ according to

$$\boldsymbol{y}_P^{(i)} = \text{vec}\left\{\mathcal{X}_P\boldsymbol{J}^{(i)}\boldsymbol{W}_T\right\} \in \mathbb{C}^{M_3 M}. \tag{2}$$

Each column of $\boldsymbol{W}_T$ is of the form

$$\boldsymbol{w}_\ell = \begin{bmatrix} 1 & e^{-j\ell\omega_0} & e^{-j2\ell\omega_0} & \dots & e^{-j(N_w-1)\ell\omega_0} \end{bmatrix}^T.$$

Here, the columns of $\boldsymbol{W}_T$ compute $M_3 \le N_w$ frequency bins centered at DC according to

$$\boldsymbol{W}_T = \begin{bmatrix} \boldsymbol{w}_{N_w-(M_3-1)/2} & \cdots & \boldsymbol{w}_0 & \cdots & \boldsymbol{w}_{(M_3-1)/2} \end{bmatrix},$$

where we have invoked the wrap-around property of the DFT matrix. Optionally, this operation may also take place in the beamspace-frequency domain. In this case, the selected correlation output is also premultiplied with $\boldsymbol{W}_S$ according to

$$\boldsymbol{y}_P^{(i)} = \text{vec}\left\{\boldsymbol{W}_S\mathcal{X}_P\boldsymbol{J}^{(i)}\boldsymbol{W}_T\right\}. \tag{3}$$

In case of a uniform linear array (ULA), the transformation from element space to beamspace is accomplished by choosing only those $L_S < M$ rows of a DFT matrix $\boldsymbol{W}_S$ of size $L_S \times M$ that encompass the sector of interest [5].

We assume that the channel stays approximately constant for at least one slot. The space-frequency SIN covariance matrix

$$\hat{\boldsymbol{R}}_{SIN} = \boldsymbol{y}_P^{(1)} \cdot \boldsymbol{y}_P^{(1)H} \tag{4}$$

is estimated by using only one space-frequency snapshot that contains the multipaths of the user of interest, cf. Figure 2. The corresponding space-frequency IN covariance matrix is estimated as [4]

$$\hat{\boldsymbol{R}}_{IN} = \frac{1}{N_s M_c - 2N_w + 1}\sum_{i=N_w}^{N_s M_c - N_w} \boldsymbol{y}_P^{(i)} \cdot \boldsymbol{y}_P^{(i)H}. \tag{5}$$

By estimating the space-frequency IN covariance matrix $\boldsymbol{R}_{IN}$ in addition to the space-frequency SIN covariance matrix $\boldsymbol{R}_{SIN}$, the signal to interference and noise ratio

$$\text{SINR} = \max_{\boldsymbol{w}} \frac{\boldsymbol{w}^H\boldsymbol{R}_S\boldsymbol{w}}{\boldsymbol{w}^H\boldsymbol{R}_{IN}\boldsymbol{w}} = \max_{\boldsymbol{w}} \frac{\boldsymbol{w}^H\boldsymbol{R}_{SIN}\boldsymbol{w}}{\boldsymbol{w}^H\boldsymbol{R}_{IN}\boldsymbol{w}} - 1 \tag{6}$$

can be maximized. The weight vector $\boldsymbol{w}$ yielding the optimum SINR for symbol decisions, cf. Section 4.2, is the "largest" generalized eigenvector of the $L_S M_3 \times L_S M_3$ matrix pencil $\{\hat{\boldsymbol{R}}_{SIN}, \hat{\boldsymbol{R}}_{IN}\}$. By transforming the covariance matrices into the space-frequency domain, noisy space-frequency bins with low signal power can be omitted, thus reducing the size of the covariance matrices and the computational complexity of (6).

Note that the space-frequency SIN covariance matrix $\hat{\boldsymbol{R}}_{SIN}$ estimated in (4) has rank one. Therefore, a scaled version of $\boldsymbol{w}$ is given by

$$\hat{\boldsymbol{R}}_{IN}\boldsymbol{w}' = \boldsymbol{y}_P^{(1)}. \tag{7}$$

Since $\hat{\boldsymbol{R}}_{IN}$ is positive definite and symmetric, we can perform a Cholesky factorization [1] of $\hat{\boldsymbol{R}}_{IN}$ and obtain $\boldsymbol{w}'$ by solving two triagonal systems. Note that the channel does not change completely from slot to slot. Therefore, an iterative scheme, e.g., the Gauss-Seidel iteration [1], would allow us to track $\boldsymbol{w}$ at reduced computational cost since the estimated weight vector of the previous slot can be used as initialization for the current slot.

[3] The correlator sequence $c_P(nT_I)$ must also take complex scrambling into account. Descrambling separates the PDCH and the PCCH.

[4] It is not necessary to use each snapshot given by $i = N_w, N_w + 1, ..., N_s M_c - N_w$. However, $\hat{\boldsymbol{R}}_{IN}$ must have full rank.

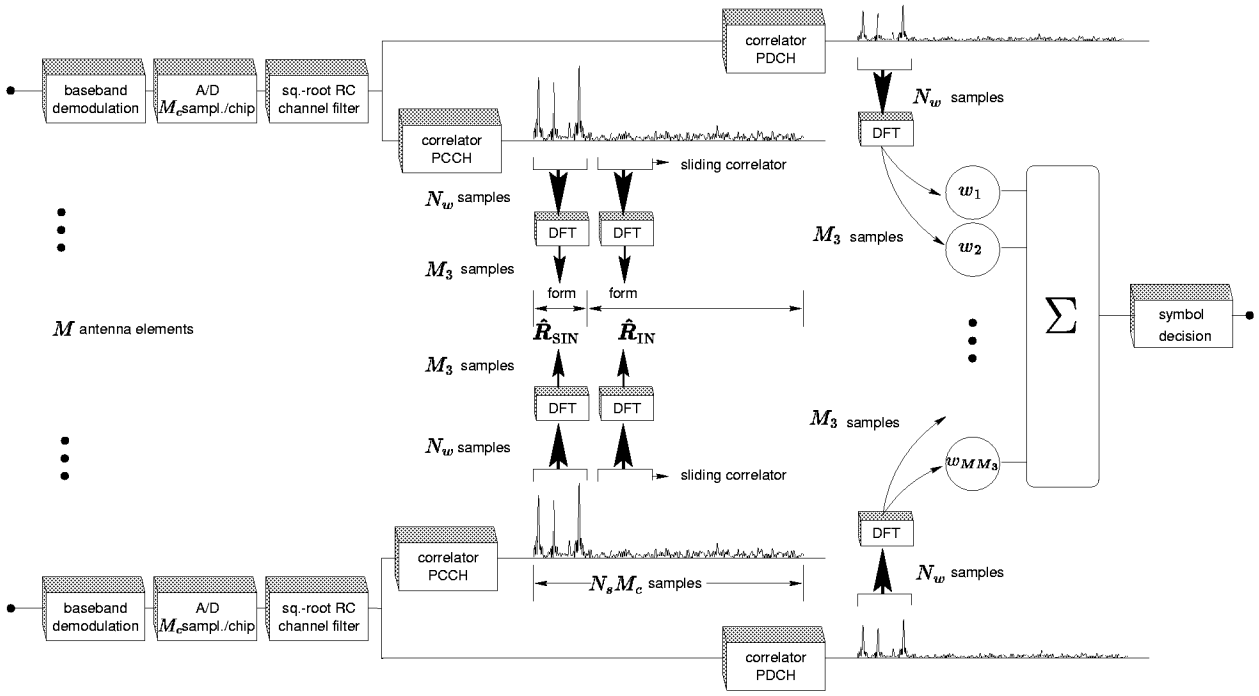

Figure 2: Structure of the space-frequency rake receiver: The N_P pilot symbols at the beginning of each PCCH slot are used to generate the space-frequency covariance matrices $\hat{\boldsymbol{R}}_{\text{SIN}}$ and $\hat{\boldsymbol{R}}_{\text{IN}}$. The "largest" generalized eigenvector $\boldsymbol{w}$, which is the optimum weight vector, is applied to the PCCH and PDCH to obtain the remaining control symbols and the data symbols, respectively.

4. RAKE RECEIVER STRUCTURES

We assume that the receiver is synchronized to the beginning of the ℓth bit in the PDCH slot.

4.1. Conventional Space-Time Rake Receiver

The searcher of a conventional rake [4] is applied to the correlator output of each antenna to estimate N_f fingers per antenna element. Each finger is characterized by its delay $g_{m,n}T_I$ and complex amplitude $w_{m,n}$, where $1 \leq n \leq N_f$ and $1 \leq m \leq M$ hold. Then the decision variables are obtained by maximum ratio combining

$$\hat{b}_D^{(\ell)} = \sum_{m=1}^{M} \sum_{n=1}^{N_f} w_{m,n}^H \cdot \mathcal{X}_D^{(\ell)}(m, g_{m,n}), \tag{8}$$

where $\mathcal{X}_D^{(\ell)}(y,x)$ denotes the y-th element in the x-th column of the matrix $\mathcal{X}_D^{(\ell)}$.

4.2. Space (Beamspace)-Frequency Rake Receiver

The (over)sampled output of each antenna element is passed through a correlator described by [5]

$$c_D(nT_I) = z_D(nT_I), \tag{9}$$

where z_D is defined in Section 2. Let each row of $\mathcal{X}_D^{(\ell)} \in \mathbb{C}^{M \times N_w}$ contain N_w samples of the output of the corresponding antenna element after the correlator. The snapshot corresponding to the ℓth bit of the PDCH slot is obtained according to (2)

$$\boldsymbol{y}_D^{(\ell)} = \text{vec}\left\{\mathcal{X}_D^{(\ell)} \boldsymbol{J}^{(1)} \boldsymbol{W}_T\right\}$$

for operation in the space-frequency domain or according to (3) for operation in the beamspace-frequency domain. The optimum decision statistic [6] may then be expressed as

$$\hat{b}_D^{(\ell)} = \boldsymbol{w}^H \cdot \boldsymbol{y}_D^{(\ell)}, \tag{10}$$

where $\boldsymbol{w}$ is the optimum weight vector defined in (6).

5. SIMULATION RESULTS

A simple four-ray multipath channel is assumed for the user of interest as well as for three interfering users. The (time-invariant) channel parameters are given in Table 1. Weaker interfering users are modeled by adding white Gaussian noise to the channel. We assume a maximum delay spread of $\tau_{\max} \approx 10\mu s$ which corresponds to 40 chips. Adjacent sensors of the base station ULA are separated by half a wavelength. Further simulation parameters are given in Figure 3.

In Figure 3 (a), the power of the first of three interfering users at the receiver is varied between 0 dB and 30 dB with respect to the power of the signal of interest. The power of the second and third interferers equals $\text{SIR}_2 = -10$ dB and $\text{SIR}_3 = -15$ dB, respectively. In contrast to the conventional space-time rake, the rakes based on the covariance matrices are near-far resistent. The beamspace-frequency rake drops the beam corresponding to interferer #1 and has the best performance. Furthermore, the space-frequency rake and the beamspace-frequency rake only use $M_3 =$

[5] The correlator sequence $c_D(nT_I)$ must also take complex scrambling into account.

multipath channel	user of interest	interferer # 1	interferer # 2	interferer # 3
wavefront # 1	(+35.4°, 30.9, 0.57)	(-81.6°, 00.0, 1.34)	(-62.0°, 12.6, 0.56)	(+46.9°, 19.4, 1.00)
wavefront # 2	(+13.3°, 08.5, 1.71)	(-82.9°, 03.7, 0.75)	(+74.5°, 32.6, 1.03)	(-59.5°, 13.7, 0.73)
wavefront # 3	(-20.4°, 19.4, 0.66)	(-71.5°, 09.3, 0.66)	(+59.6°, 30.1, 0.71)	(-88.3°, 09.9, 0.57)
wavefront # 4	(-26.4°, 35.4, 1.52)	(+71.4°, 04.3, 0.98)	(-31.1°, 20.4, 1.04)	(+82.9°, 39.5, 0.73)

Table 1: The user of interest and three interferers are modeled by a simple four-ray multipath channel. Each ray is characterized by its angle of arrival with respect to the boresight of the base station ULA in degrees, by its delay in chips, and by its attenuation - the table contains the absolute values of the complex attenuations.

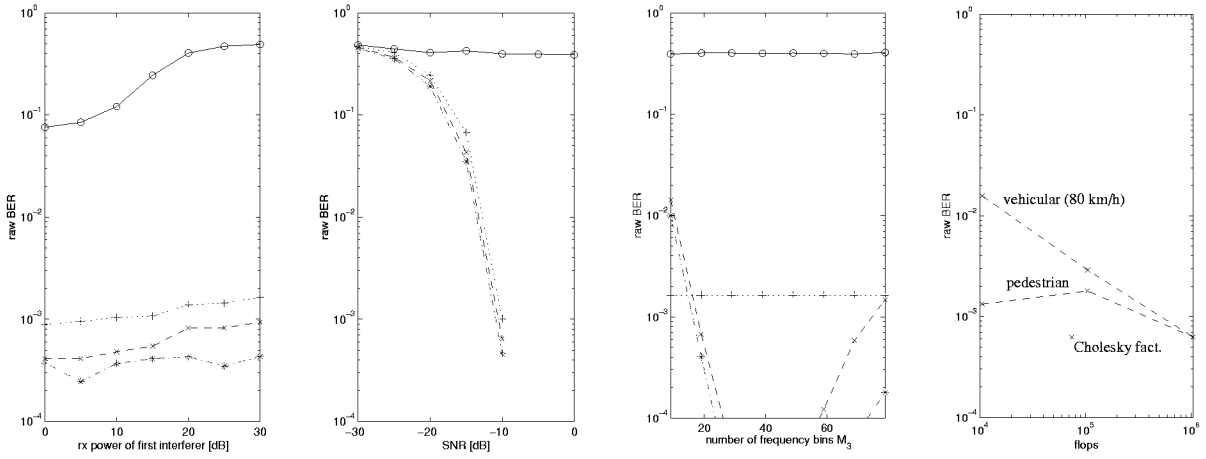

Figure 3: The conventional space-time rake, the space-time rake, the space-frequency rake, and the beamspace frequency rake are denoted by 'o', '+', 'x', and '*', respectively. The performance criterion is the raw bit error rate (BER) averaged over 2000 slots. Figure (a) shows the performance as a function of the power of the first interfering user at the receiver in relation to the power of the user of interest in dB. Figure (b) indicates the influence of noise in relation to the power of the user of interest in dB. The performance as a function of the number of frequency bins M_3 is shown in Figure (c). If not stated otherwise, the following parameters hold: $M_c = 2, N_w = 79, M_3 = 19, M = 4, L_S = 3, \text{SNR} = -10$ dB, $\text{SIR}_1 = -20$ dB, $\text{SIR}_2 = -10$ dB, $\text{SIR}_3 = -15$ dB, $n_D = 128, n_C = 256, N_P = 6, N_f = 3$. Figure (d) shows the performance of the space-frequency rake as a function of the provided computational power to calculate the optimum weight vector either iteratively or by Cholesky decomposition for two time-variant channels. Here, we used one instead of three interfering users. Following parameters have changed: $M_3 = 9, \text{SNR} = 0$ dB, $\text{SIR}_1 = -10$ dB.

19 out of $N_w = 79$ frequency bins. They perform slightly better at a significantly reduced computational complexity than the space-time rake. Figure 3 (b) indicates the influence of noise in relation to the power of the user of interest in dB. The frequency bins centered around DC have more signal energy. Therefore, weaker frequency bins can be omitted. Due to noise effects, the performance may increase if the weaker frequency bins are not considered, cf. Figure 3 (c). For the simulations plotted in Figure 3 (d), we used a slow (pedestrian) and a fast (vehicular) time-variant channel including scatterers. The performance of the space-frequency rake for 1, 10, and 100 Gauss-Seidel iteration steps and for the Cholesky factorization is given as a function of the flops used to determine the optimum weight vector for each slot ($T_{\text{slot}} = 0.625$ms). We see that one iteration is sufficient for slow mobiles whereas more iterations increase the performance for fast mobiles. Notice, however, that (in this setting) 10 iterations and more are computationally more complex than the Cholesky factorization, which yields the better performance.

6. CONCLUDING REMARKS

In this paper, we have presented the space-frequency (and the beamspace-frequency) rake for uplink data detection with adaptive antennas in WCDMA. The covariance matrices required for near-far resistant multi-user interference suppression are estimated by taking the uplink channel structure of WCDMA into account. The optimum weight vector may then be obtained by Cholesky factorization or by updating iteratively, thus ensuring excellent performance and real-time applicability.

If desired, the channel parameters in terms of delays, DOAs, and complex amplitudes can be estimated [2] based on the space-frequency covariance matrices for downlink beamforming or (emergency) localization.

7. REFERENCES

[1] G. H. Golub and C. F. van Loan, *Matrix Computations*, Johns Hopkins University Press, Baltimore, MD, 2nd edition, 1989.

[2] M. Haardt, C. Brunner, and J. A. Nossek, "Efficient high-resolution 3-D channel sounding", in *Proc. 48th IEEE Vehicular Technology Conf. (VTC '98)*, pp. 164–168, Ottawa, Canada, May 1998.

[3] E. Nikula, A. Toskala, E. Dahlman, L. Girard, and A. Klein, "FRAMES Multiple Access for UMTS and IMT-2000", *IEEE Pers. Comm. Mag.*, Apr. 1998.

[4] J. G. Proakis, *Digital Communications*, McGraw-Hill, New York, NY, 2nd edition, 1989.

[5] M. D. Zoltowski, M. Haardt, and C. P. Mathews, "Closed-form 2D angle estimation with rectangular arrays in element space or beamspace via Unitary ESPRIT", *IEEE Trans. Signal Processing*, vol. 44, pp. 316–328, Feb. 1996.

[6] M. D. Zoltowski, J. Ramos, C. Chatterjee, and V. Roychowdhury, "Blind adaptive 2D rake receiver for DS-CDMA based on space-frequency MVDR processing", *IEEE Trans. Signal Processing*, June 1996, submitted for publication.